OPTIMIZATION OF GEOTHERMAL POWER PLANT DESIGN FOR EVOLVING OPERATING CONDITIONS

Mathieu Pollet, Louis Gosselin*, Jonathan Dallaire, François Mathieu-Potvin

Department of Mechanical Engineering, Université Laval, Québec City, Québec, Canada, G1V 0A6

Article accepté pour publication dans : Applied Thermal Engineering, Volume 134, April 2018.

Abstract

The main goal of this work is to determine optimal geothermal power plant designs by taking into account the transient evolution of the plant/reservoir system. To do so, a geothermal reservoir model is developed, where the permeability of the ground is represented by a series of parallel pipes inside which the underground water can flow. The reservoir model is coupled to an evolving Organic Ranking Cycle (ORC), where the pressure at the condenser adapts to the conditions in the geothermal reservoir (temperature of the brine and mass flow rate) based on the Stodola equation. The system is then optimized in order to maximize the total energy output of the power plant over its lifetime. A series of parametric analyses was performed for relevant design parameters (e.g., overall conductance of the heat exchanger at the evaporator, turbine sizes, number of years of operation, etc.), while other parameters were optimized, namely the working fluid to geofluid mass flow rate ratio, the pressure at the evaporator, and the geofluid mass flow rate. The optimal values that were found were values that yielded viable cycles over the entire exploitation period of the plant and that did not deplete the thermal reservoir prior to the end of the plant lifetime. ORC cycles that were optimized by considering the time evolution of the system were then compared against cycles optimized under the assumption of constant geothermal reservoir properties. It was also demonstrated that by allowing key design parameters to change over the course of the exploitation of the plant, it was possible to further increase the plant performance.

* Corresponding Author: Louis.Gosselin@gmc.ulaval.ca; Tel.: +1-418-659-7829; Fax: +1-418-659-5343

Keywords: geothermal power plant; geothermal reservoir model; optimization; organic Rankine cycle (ORC);

Nomenclature

a	reservoir volume parameter, $c_{pf}/\rho c_{pr} V_{res}$ (1/kg)
b	reservoir heat transfer parameter, $ph_{conv} N_p L/c_{pf}$ (kg/s)
c_p	specific heat (J/kg K)
E	energy produced (W h)
H	height (m)
h	enthalpy (kJ/kg)
h_{conv}	convection coefficient (W/m^2 K)
K	turbine constant (kg K$^{1/2}$/s MPa)
L	length (m)
$\dot{m}$	mass flow rate (kg/s)
N	lifetime (year)
N_p	number of "pipes" in the reservoir model
n	year considered
P	pressure (Pa)
P_{high}	pressure at the evaporator (Pa)
p	perimeter (m)
q	heat transfer rate (W)
r	working fluid to geofluid mass flow rate ratio
s	entropy (J/kg K)
T	temperature (K)
T_{cond}	temperature at the condenser (K)
t	time (s)
UA	evaporator conductance (W/K)
V	volume (m^3)
W	power (W)
x	position (m)

Greek Symbols

Δt	time step (s)
ΔT_{lm}	logarithmic mean temperature difference (K)
η	efficiency
ρ	density (kg/m^3)

Subscripts

1-7	working-fluid states
A-D	geofluid states
d	design
f	fluid
gen	property of the electric generator
geo	geofluid
in	inlet
max	maximum
off	off-design
opt	optimized
out	outlet
p	pipe
planned	planned with steady state conditions
pump	property of the pump
r	rock
res	reservoir
s	isentropic
tot	total
turb	property of the turbine
wf	working-fluid

1. Introduction

Deep geothermal energy is among the most promising sources of renewable energy and it can serve as a base load power generating source [1]. Although the resource is abundant,

only a small fraction of it is viable for most engineering applications. The progress in drilling technologies and the reduction of drilling costs, however, facilitate the access to an increasing number of deep geothermal reservoirs [2]. As a consequence, more and more countries are currently considering the potential of geothermal energy to complement their energy portfolio. In fact, according to the technology roadmap for geothermal heat and power published by the International Energy Agency, geothermal electricity generation could reach around 3.5% of the global electricity production by the end of 2050, avoiding nearly 800 megatons of CO_2 emissions per year [3].

It is of crucial importance to evaluate the sustainability of geothermal energy technologies and the overall environmental impact of this energy source [4–6]. Indeed, available historical data shows that over the course of their exploitation, the temperature, pressure, enthalpy, and/or brine flow rates of the geothermal reservoirs generally decrease [7–10]. This is mostly explained by the reinjection of the cold brine in the reservoir over the lifespan of the power plants. For particularly long operation periods, the depletion of the geothermal reservoirs may result in severe performance drop, as the plants will operate mostly under off-design conditions [11]. Nevertheless, in most of the studies found in literature, the thermal reservoir properties (geofluid temperature and mass flow rate) are assumed constant for the entire lifetime of the plants. This approach was used, for example, in recent work by Heberle et al. [12], where the authors present a study on geothermal power generation by binary power plants based on representative geothermal conditions in Germany. The authors considered the cases of the Southern German Molasse Basin and the Upper Rhine Rift Valley and used geothermal parameters corresponding to average properties in each region. By considering different geothermal power plants concepts, they showed that using low Global Warming Potential (GWP) working fluids could yield equivalent second law efficiency [13] and significantly lower environmental impact (global warming impact, demand on finite energy resources, eutrophication, and acidification) as compared to common fluorinated working fluids.

Another type of problems for which constant geothermal properties are often assumed is the optimization of geothermal power plant performance, i.e., thermal efficiency, exergy analysis, cost, etc. In these studies, the power plant designs are often optimized in a steady-state regime under the assumption that the geothermal fluid

properties are equal to their initial values for the duration of the analysis. For example, Barse and Mann [14] compared constrained and unconstrained system designs for a basic Organic Rankine Cycle and a total of twelve working fluids. Their numerical model was validated with the Chena geothermal power plant (built at Chena Hot Springs in Alaska, USA) and used constant values for both geothermal fluid temperature and mass flow rate. The authors showed that, depending on the choice of the working fluid, optimizing the system could lead to an increase in thermal efficiency as high as 25% and a decrease in Levelized Cost of Electricity (LCOE) as low as 11%. Hettiarachchi et al. [15] minimized the ratio of the heat exchanger area to the net power output of geothermal ORC power plants, under a steady-state assumption with a brine temperature of 90°C. Values from 0.35 to 1.26 m^2/kW were obtained depending on the working fluid. Ergun et al. [16] performed a exergoeconomic analysis of an ORC geothermal power plant located in Turkey. They showed that the evaporator is the piece of equipment responsible for the highest exergy destruction. They also achieved a unit cost of the electricity produced of 7.96$/GJ. Similarly, Zare [17] performed a comparative exergoeconomic analysis for different geothermal power plant designs. They considered three different configurations, namely a simple ORC, a regenerative ORC, and an ORC with internal heat exchanger. In each analysis, the authors assumed that the systems operated in steady-state conditions. Different values were considered for the geothermal fluid properties, but they were kept constant in all scenarios. The author concluded that, among the cycles considered, the ORC with internal heat exchanger and the simple ORC offered superior performance from thermodynamic and economic perspectives, respectively.

More recently, a certain number of studies were performed by considering the geothermal resource degradation over time. In fact, even though they considered a steady-state model, Liu et al. [18] demonstrated the impact of the heat source temperature on the performance of a geothermal power plant, which reinforces the idea of considering the entire plant lifetime when designing a cycle. Different approaches have been considered in order to model the dynamic aspects of power plants (e.g., [19], [20]), and in particular the depletion of the geothermal resource. For instance, Gabbrielli [11] assumed that the temperature of the reservoir decreased by 1ºC per year during the plant operative life and increased the geothermal fluid mass flow rate in order to keep the power plant's

thermal input constant. Using a detailed off-design simulation model for the ORC power plant, the author demonstrated that under these specific operating conditions, the best economic performance is obtained when using the temperature of the geothermal well at the end of its exploitation (i.e., the lowest temperature) instead of using the temperature at the beginning. Didit et al. [21] assumed a constant injection mass flow rate and used a curve fitting of the analytical expression for the reservoir temperature presented in [22]. Under these modeling assumptions, the authors showed that the temperature decrease of the reservoir affects both the working fluid mass flow rate and the power output of the plant. Another possible approach is to use historical data of existing thermal reservoirs, which was done by Budisulistyo et al. [23] in their study on lifetime design strategy for binary geothermal plants. The authors used data for the Wairakei geothermal resource located in the Taupo Volcanic Zone in New Zealand. Among the different results obtained in their study, the best lifetime design point was at year 7 (for a 30 years operation period).

In real design scenarios, however, only the initial properties of a thermal reservoir can generally be estimated, since the transient evolution of its properties depends on the exploitation of the geothermal power plant. The literature regarding optimization of geothermal plants including the coupling between plant designs/exploitation parameters and the reservoir is limited. In this paper, an integrated approach to the optimization of geothermal power plants is presented, where a fully coupled model between the plant and the thermal reservoir is developed. To achieve this coupling, a simple geothermal reservoir model is introduced. In addition, an optimization methodology is proposed to design a geothermal power plant by taking into account not only the evolving conditions in which the plant operates, but also the evolution of the geothermal reservoir.

The paper is organized as follows: Section 2 introduces the mathematical modeling of the geothermal reservoir and of the power plant itself. A reference case is discussed in Section 3, where typical results obtained with the model are presented and the design space is analyzed. The strategy used for the optimization of the design of the geothermal plant is described in Section 4, while the results are discussed in Sections 5-7.

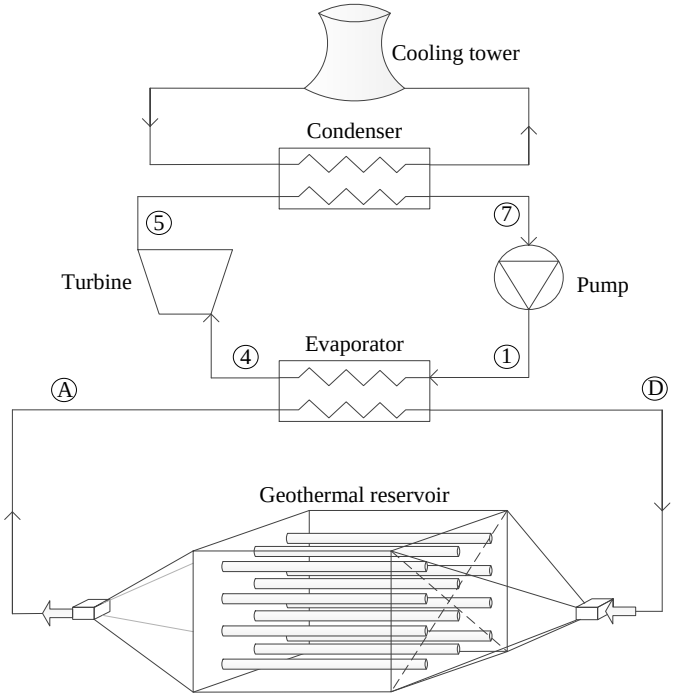

Figure 1

2. Modeling of the geothermal power plant

Consider an ORC geothermal power plant exploiting an Enhanced Geothermal System (EGS) reservoir as shown in Fig. 1. Note that, in general, EGS reservoirs encountered in deep geothermal energy applications are located several kilometers underground, as opposed to vertical ground heat exchangers used for building heating and/or cooling, which most of the time reach depths of only a few hundred meters. A fluid (herein called "geofluid") is injected in the reservoir through a borehole (injection well) and recollected a few hundred meters away in another borehole (production well). As the geofluid circulates through the permeable fractures and porosities connecting the boreholes, it warms up. The geofluid is then used as a heat source in the geothermal power plant. Heat is extracted from the geofluid in the plant by heat exchangers that evaporate a working fluid. The cold geofluid is then pumped back in the reservoir to collect more heat, while the working fluid expands through a turbine to produce work. The working fluid is then cooled down and condensed, before being pumped at a higher pressure and circulated back in the evaporator. An example of the T-s diagram of the working fluid cycle is shown in Fig. 2. This type of cycle (i.e., Organic Rankine Cycle) was chosen among

others for its relatively high efficiency at low temperatures as those found in deep boreholes in Eastern Canada (i.e., below 125°C) [24].

A model was developed to calculate/predict the performance of the power plant with respect to the operating conditions. The overall model is made of two coupled sub-models: the first for the geothermal reservoir and the second for the power plant itself. The temperature of the geofluid at the outlet of the reservoir from the first sub-model becomes the inlet temperature of the geofluid in the power plant model and vice versa, as shown previously in Fig 1.

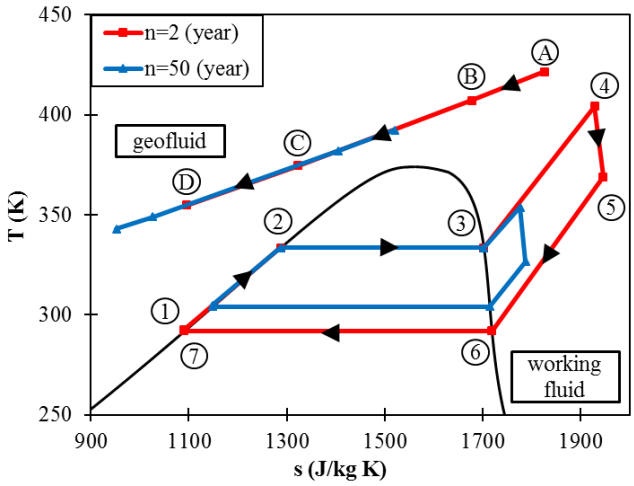

Figure 2

2.1 Geothermal reservoir model

This subsection describes the geothermal reservoir model. The goal of this sub-model is to determine the time evolution of the temperature of the geofluid at the reservoir outlet (i.e., at state A in Fig. 1) as a function of the inlet temperature, geofluid mass flow rate and properties of the reservoir (e.g., conductivity, initial temperature, dimensions, etc.). Since the focus of the present work is on the power plant itself, only a simplified representation of the reservoir was used here. Future work could include a more refined hydrogeological model.

The reservoir is represented as a large "box" with a section H×H and a length L. The actual depth (distance underground) of the geothermal reservoir is not specified at this point, as heat gains/losses through the vertical part of the injection and production wells are neglected, i.e., only the heat gained by the geofluid when going through the

reservoir is considered in the model. To represent the enhanced permeability of the reservoir, a series of fractures or small "pipes" of perimeter p connecting the two sides of the reservoir was considered, as shown in Fig. 1. This representation of the reservoir allows analysing the heat transfer along a single "pipe" and then generalising the result to the entire reservoir since the thermal mechanisms are the same for all fractures. Assuming a uniform temperature of the volume surrounding the pipe, a heat balance on the geofluid yields:

$$\frac{\dot{m}_{geo}}{N_p} c_{pf} \frac{dT_f(x)}{dx} = p h_{conv} (T_{res}(t) - T_f(x)) \quad (1)$$

where N_p is the number of "pipes" or fractures in the reservoir and $\dot{m}_{geo}$ is the total mass flow rate of geofluid in the reservoir. Therefore, $\dot{m}_{geo}/N_p$ is the mass flow rate in a single equivalent "pipe". Eq. (1) can be integrated in the x direction in order to determine the temperature of the geofluid at the outlet of the reservoir, i.e., at x = L. The solution to Eq. (1) is:

$$T_{f,out} = (T_{f,in} - T_{res}) e^{-b/\dot{m}_{geo}} + T_{res} \quad (2)$$

where b is one of the reservoir parameters and is equal to $p h_{conv} N_p L / c_{pf}$.

Similarly, a heat balance can be performed on the reservoir itself to obtain an equation describing the evolution of the reservoir temperature:

$$\rho c_{pr} V_{res} \frac{dT_{res}}{dt} = \dot{m}_{geo} c_{pf} \left(T_{f,in} - T_{f,out}\right) \quad (3)$$

Combining Eqs. (2) and (3), one finds:

$$\frac{dT_{res}}{dt} + a\dot{m}_{geo} \left(1 - e^{-b/\dot{m}_{geo}}\right) T_{res} = a\dot{m}_{geo} \left(1 - e^{-b/\dot{m}_{geo}}\right) T_{f,in} \quad (4)$$

where the following shorthand variable has been introduced:

$$a = \frac{c_{pf}}{\rho c_{pr} V_{res}} \quad (5)$$

In the end, the physical features of the geothermal reservoir are thus represented by the two variables a and b. In the model used in this work, Eq. (4) has been solved numerically using finite differences.

It is important to note that the present reservoir model is a simplistic representation of the hydrogeological mechanisms in real reservoirs, which is used here to illustrate the proposed plant optimization framework. Much more evolved geological

and hydrogeological models and studies on specific reservoirs can be developed, see [25] for example.

2.2 Power plant model

The geothermal power plant considered in this paper uses a subcritical organic Rankine cycle as shown in Fig. 2. The decision to focus on subcritical ORCs was based on the fact that it is the most common type of ORC cycles and often more practical than others thanks to the lower pressure levels involved. Note that two different thermodynamic cycles are shown in this figure representing two different years of operation of the geothermal power plant (this will be discussed in details in the following sections). Heat from the geofluid is transferred to the working fluid in the evaporator (states 1 to 4, Fig. 2) before the geofluid is returned to the reservoir. The evaporator was separated into three parts to avoid impossible temperature crossing: from state 1 to 2 (economizer), the working fluid reaches the state of saturated liquid; from state 2 to 3, the evaporation takes place; and from state 3 to 4, the working fluid is superheated. The size of the evaporator is characterized by a total value of UA, which for the purpose of this paper is considered to be the summation of the UA-value of the three parts of the heat exchanger:

$$\mathrm{UA_{tot}} = \mathrm{UA_{1-2}} + \mathrm{UA_{2-3}} + \mathrm{UA_{3-4}} \tag{6}$$

In the present work, the value of UA_{tot} is specified before the cycle performance is evaluated because the size of the evaporator is considered fixed during the power plant lifetime. However, the repartition of UA_{tot} between the three parts of the evaporator needs to be determined (i.e., $UA_{1\text{-}2}$, $UA_{2\text{-}3}$ and $UA_{3\text{-}4}$). For a given pressure in the evaporator, an initial guess for state 1 is made, while states 2 and 3 are known. Therefore, provided that UA_{tot} is also known, only state 4 is to be found.

In order to do so, a guess on the value of the geofluid temperature at the outlet of the evaporator (T_D) is made to begin the iterative calculation. One can then determine the required UA value from state 1 to 2 as follow (See Chapter 11.3 in Ref. [26]):

$$\mathrm{UA_{1\text{-}2}} = \frac{\mathrm{q_{1\text{-}2}}}{\Delta \mathrm{T_{lm1\text{-}2}}} = \frac{\dot{\mathrm{m}}_{\mathrm{wf}}(\mathrm{h_2} - \mathrm{h_1})}{\Delta \mathrm{T_{lm1\text{-}2}}} \tag{7}$$

State C of the geofluid is found from an energy balance in the economizer:

$$\mathrm{h_C} = \frac{\dot{\mathrm{m}}_{\mathrm{wf}}}{\dot{\mathrm{m}}_{\mathrm{geo}}}(\mathrm{h_2} - \mathrm{h_1}) + \mathrm{h_D} \tag{8}$$

A similar procedure can be applied from states 2 to 3, yielding:

$$UA_{2\text{-}3}=\frac{q_{2\text{-}3}}{\Delta T_{lm2\text{-}3}}=\frac{\dot{m}_{wf}(h_3-h_2)}{\Delta T_{lm2\text{-}3}} \quad (9)$$

$$h_B=\frac{\dot{m}_{wf}}{\dot{m}_{geo}}(h_3-h_2)+h_C \quad (10)$$

After these steps, all the thermodynamic states of the geofluid and of the working fluid are known, except state 4 of the working fluid. The heat transfer rate in the superheater is determined from a heat balance in the geofluid, which allows finding state 4:

$$h_4=\frac{\dot{m}_{geo}}{\dot{m}_{wf}}(h_A-h_B)+h_3 \quad (11)$$

The required UA-value in the superheater is thus:

$$UA_{3\text{-}4}=\frac{q_{3\text{-}4}}{\Delta T_{lm3\text{-}4}}=\frac{\dot{m}_{wf}(h_4-h_3)}{\Delta T_{lm3\text{-}4}} \quad (12)$$

Finally, the total UA value is calculated by summing the three contributions mentioned above, i.e., Eqs. (7), (9) and (12), and is compared to the specified UA_{tot}. The difference between the calculated and specified values of UA_{tot} is minimized with the function *fzero* from the optimization toolbox in Matlab [27] by changing the value of T_D. Convergence is declared when T_D varies by less than 10^{-3} % between two consecutive iterations. Note that the pinch point may occur at different locations in the evaporator (between states 1-A, 2-C, 3-B, or 4-A). All possible pinch points are systematically verified while solving for the unknown temperatures in the evaporator. When unphysical temperature crossings occur, the guess of T_D is updated (i.e., slightly increased) and the iterative procedure is restarted. This process is repeated until the guess of T_D allows solving for all unknown temperatures in the evaporator without any temperature crossings in the heat exchanger. In addition, a constraint is imposed on T_D in order to avoid silica scaling when the geofluid is returned in the ground: more specifically, when T_D is too small (e.g., below 30°C), the plant design is rejected. Note that in practice the specific value of the minimal reinjection temperature depends on the properties of the geological environment. For the type of reservoir considered in this study, reinjection fluid temperature generally varies between 50 °C and 100 °C [28]. A slightly lower value is used for the constraint on T_D only to facilitate the convergence of the *fzero* function. However, in all simulations, the

reinjection temperature was verified and found to be within the range $65\ °C \leq T_D \leq 100\ °C$.

In the process of determining the repartition of UA_{tot} between the three subparts of the evaporator, it is possible that the specified overall UA value is not high enough to superheat the working fluid, depending on the values of the different design variables and parameters (pressure, flow rate, etc.). In other words, the state of the working fluid at the exit of the evaporator might fall under the saturation curve or at the left of the saturation curve in the T-s diagram (compressed liquid). The designs corresponding to this situation were eliminated in the present model. Note that the high pressure P_{high} of the power cycle (i.e., $P_{high} = P_1 = P_2 = P_3 = P_4$) is considered in the present model as a design variable of the power plant. This means that the model and calculation procedure consider that this value is known, but as will be described in Section 3, the high pressure value will be varied to optimize the power cycle performance.

Once state 4 is positioned, the working fluid enters the turbine. The outlet point (state 5) of the turbine was assumed to be governed by the Stodola equation [29]. According to that relation, depending on the working fluid mass flow rate and pressure at the inlet of the turbine, the pressure at the exit is:

$$P_5 = \sqrt{P_4^2 - \dot{m}_{wf}^2 \frac{T_4}{K^2}} \tag{13}$$

where K is the turbine constant. This constant is the slope on the linear characteristic of turbine performance. It takes into account the size and quality of the turbine. The turbine is also characterized by its second-law efficiency:

$$\eta_{turb} = \frac{h_4 - h_5}{h_4 - h_{5,s}} \tag{14}$$

where $h_{5,s}$ is the enthalpy of the working fluid considering an isentropic turbine. Provided that the efficiency is known, the actual position of state 5 is calculated from Eq. (14) (see Chapter 7 in [30]). However, the information that is usually known is the efficiency in specific “design conditions”. In order to consider situations where the turbine is operating outside of the conditions for which it has been designed, its off-design behaviour needs to be taken into account. The model of Ref. [11] was retained, in which the off-design

efficiency is obtained from the design efficiency, multiplied by a correction factor taking into account variations of volume flow rates with respect to the design conditions:

$$\eta_{turb,off}=\eta_{turb,d}\sin\left[0.5\pi\left(\frac{\dot{m}_{wf\text{-}in\text{-}off}}{\dot{m}_{wf\text{-}in\text{-}d}}\frac{\rho_{wf\text{-}in\text{-}d}}{\rho_{wf\text{-}in\text{-}off}}\right)^{0.1}\right] \quad (15)$$

It is the efficiency $\eta_{turb,off}$ that is used in Eq. (14) to calculate enthalpy at state 5. In order to avoid the presence of liquid droplets in the turbine which would affect its efficiency and lifetime, a constraint was imposed to state 5, i.e., it could only be a saturated or superheated vapor. Designs that yielded saturated liquid-gas mixtures for state 5 were rejected.

The last part of the power cycle model includes the cooling of the working fluid in the condenser right after the turbine. In the condenser, the working fluid begins to condense at point 6 and reaches the saturated liquid state at point 7, see the T-s diagram in Fig. 2. Finally, the working fluid is pumped to a higher pressure between states 7 and 1. The second law efficiency of the pump is:

$$\eta_{pump}=\frac{h_{1,s}-h_7}{h_1-h_7} \quad (16)$$

State 1 determined from Eq. (16) and the initially assumed state 1 should then be compared. An iterative procedure was implemented to repeat the procedure described in the present section until convergence is reached, i.e., when the difference of enthalpy at state 1 is less than 0.01% between two consecutive iterations.

The model described in this sub-section was implemented numerically, including the iterative procedures mentioned above. The known parameters required to simulate the cycle are: (i) UA_{tot}, (ii) the high pressure P_{high}, (iii) the geofluid mass flow rate $\dot{m}_{geo}$, (iv) the working fluid mass flow rate $\dot{m}_{wf}$, (v) the working fluid (i.e., its thermodynamic properties), (vi) the turbine parameter K and (vii) its design efficiency $\eta_{turb,d}$, (viii) the geofluid conditions (temperature, pressure) at the inlet of the plant, and (ix) the pump efficiency η_{pump}. The output of the model is the thermodynamic properties at each state of the cycle that result from the given set of known parameters mentioned above, which in turn, allows calculating the power output of the cycle:

$$W_{turb}=\dot{m}_{wf}(h_4-h_5) \quad (17)$$

as well as the geofluid temperature at the outlet of the power plant (i.e., reinjection temperature at state D).

In order to validate the power plant model developed in this paper, results were compared to those published by Chagnon-Lessard et al. [31] for an ORC working in steady-state conditions, i.e., with a constant geofluid temperature. Therefore, the specific power output of the power plant at the first time step of the present model were calculated for different condensing temperatures and geofluid temperatures, and then compared to the values obtained from the model of Ref [31]. Differences were below 7% on average for the cases tested. The discrepancies come from the differences in the turbine and heat exchanger models, as well as in the software used to calculate the working fluid properties. Given the small range of discrepancies, the implementation of the present power plant model was thus considered to be verified and adequate.

2.3. Coupling of the two submodels

Section 2.1 described the geothermal reservoir model which allows calculating the temperature of the geofluid at the inlet of the power plant, while Section 2.2 presented the power plant model which returns the temperature of the geofluid before it is reinjected in the reservoir. Section 2.3 explains how the two submodels were coupled in a time-stepping procedure.

To estimate the initial condition of the system, a guess was made for the inlet temperature of the geofluid in the reservoir ($T_{f,in}$) and the temperature of the geofluid exiting the reservoir ($T_{f,out}$) was determined from Eq. (2). This temperature was then used as an input for the second submodel ($T_A=T_{f,out}$) to calculate the cycle performance, which allowed making a new estimation of the geofluid temperature at the outlet of the plant (i.e., T_D, which becomes the new estimation of $T_{f,in}$). It was then compared to the previous guess and an iterative procedure was implemented to update the value of $T_{f,in}$ (i.e., the calculated value of $T_{f,in}$ at the end of an iteration becomes the guess for the new iteration). Convergence was declared when the temperature difference between two consecutive iterations was less than 1%.

Then, for the other time steps, the value of T_D at the previous time step was used as the initial guess for $T_{f,in}$ to start the iterative procedure described in the previous

paragraph. When the state of the entire system is solved for a time step, the new reservoir temperature is calculated by using Eq. (4). A time-step of 1 year was used in the present work (assuming an average of 30 days each month).

3. Reference case and design space

A reference case is first presented to illustrate the typical results achieved by the model. The geofluid was water and the reservoir was initially at 150°C. The working fluid in the ORC was R134a. This working fluid was selected based on the work of Ref. [31], which identified optimal working fluids as a function of the brine temperature for subcritical and transcritical ORCs. The mass flow rates and evaporator pressure were constant during the lifetime of the system. The mass flow ratio between the geofluid and the working fluid

$$r = \frac{\dot{m}_{geo}}{\dot{m}_{wf}} \tag{18}$$

was fixed to 1 (this ratio will be optimized later). The values of the parameters used to simulate this reference case are listed in Table 1 below. A sensitivity analysis was performed for both reservoir parameters a and b. It was found that small values of a (e.g., large geothermal reservoir, large amounts of heat stored in the reservoir, etc.) linearly increased the amount of energy that the power plant could produce during its exploitation period, and vice-versa. The constant of proportionality varied depending on the different parameters and operating conditions of the ORC. On the other hand, large values of the parameter b (e.g., large heat transfer exchange surface in the reservoir, high heat transfer coefficient in the fractures, etc.) yielded the highest amount of energy produced by the plant. In fact, very large values of b resulted in a geofluid temperature at the outlet of the reservoir that was equal to the reservoir temperature. On the opposite, very small values of b resulted in a nearly constant geofluid temperature as it traveled through the reservoir and, consequently, greatly diminished the energy that was produced by the plant. In the simulations performed in this study, b was large enough so that the geofluid temperature at the outlet of the reservoir was close to equal to the reservoir temperature at every time step.

Table 1. Values of the model parameters for the reference case.

Parameter (units)	Value
UA_{tot} (kW/K)	100
K (kg $K^{1/2}$/s MPa)	200
$\eta_{turb,d}$ (-)	0.8
η_{pump} (-)	0.9
η_{gen} (-)	0.9
a (1/kg)	2.09×10^{-11}
b (kg/s)	2051
Initial T_{res} (°C)	150
N (year)	50

To illustrate what the design space looks like, a parametric sweeping over two design variables was performed, namely the evaporator pressure and the geofluid mass flow rate. For each possible set of these two design variables, the model presented above was used to evaluate the energy produced over the lifetime of the power plant:

$$E_{tot}=\sum_{n=1}^{N}\left[E_{turb}(n)-E_{pump}(n)\right]=\sum_{n=1}^{N}\left[\dot{m}_{wf}(h_4-h_5)\eta_{gen}-\dot{m}_{wf}(h_1-h_7)\right]\Delta t \qquad (19)$$

where η_{gen} is the efficiency factor for the electric generator using the mechanical power exiting the turbine which was fixed to 0.9 in this study.

The evaporator pressure was allowed to vary between 1 and 4 MPa (corresponding to the critical pressure of the working fluid) by incremental steps of 0.1 MPa and the geofluid flow rate, from 6 to 50 kg/s by steps of 1 kg/s. Combinations of pressures and flow rates for which no viable cycles existed were assigned a value of 0 for the energy production. Results of this parametric study are reported in Fig. 3. An optimal design is clearly visible in the figure; it is achieved with a pressure of ~1.7 MPa and a flow rate of ~16 kg/s, leading to a maximized energy production of 113.9 GWh. Note that, due to the choice of the incremental steps for each variable when performing the

parametric sweeps, there could be designs that yield slightly better energy production, as will be shown in the upcoming sections.

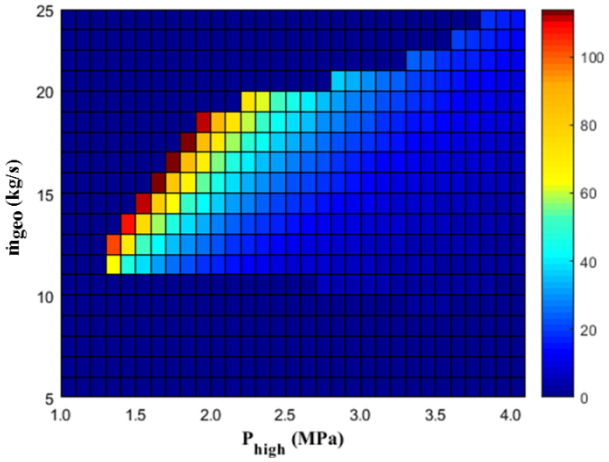

Figure 3

It can be seen in Fig. 3 that the viable design space is essentially constrained by three limiting factors and thus, exhibits a triangular shape. The lower edge of the design space is delineated by the constraint imposed on the geofluid reinjecting temperature which was introduced above. This happens when there is not enough energy available in the geofluid to supply the power plant. Furthermore, when the geofluid mass flow rate is too small, the reinjection temperature could become too low. The upper edge of the triangle is generated by the turbine model, Eq. (12). With larger mass flow rates, the point 5 of the power cycle can fall inside the bell-shape in the T-s diagram (i.e., gas-liquid mixture) or can have too low a pressure, which eliminates the design in the present approach. Finally, the right-hand side edge of the design space is due to the fact that only subcritical cycles have been modeled, when the pressure becomes higher than the critical pressure (4.06 MPa for R134a), the cycle is eliminated.

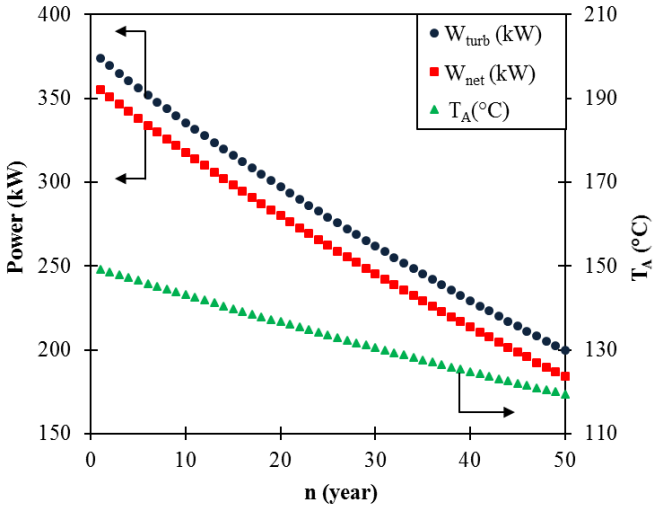

Figure 4

In addition to the design space, it is interesting to observe the difference in the power cycle itself from the beginning of the exploitation to the end of life, for the optimal design seen in Fig. 3. As seen in Fig 2 (which shows the T-s diagram for this specific cycle) the cooling of the reservoir over the lifetime of the project tends to decrease the temperature of point 4. As a consequence, the pressure drop in the turbine is less important (see Eq. (13)), and the entire cycle becomes "thinner" when represented in a T-s diagram and produces less power as time goes by. The decrease of performance can be directly correlated to the geofluid temperature drop. The geofluid temperature entering the power plant falls from 150ºC to less than 120ºC during the lifetime of the plant with the current settings, whereas power produced decreases from 360 kW initially to 178 kW at the end of the project, see Fig. 4. Since the pumping power is almost constant in time, whereas the power produced by the turbine declines, the relative importance of the pumping energy increases in time. Pumping represents 5% of the energy produced by the turbine initially, and this fraction reaches 7.8% at the end of the plant lifetime.

4. Optimization approach

The previous sections described the model itself and the type of results that it can yield. The test case studied in Section 3 revealed optimization opportunities to maximize the energy production over the power plant lifetime, considering the changes in the reservoir

temperature. In the next sections, these optimization opportunities will be rigorously addressed. In order to do so, a more practical method than the parametric sweep described in Section 3 is required. Therefore, the optimization problem will be formulated in the present section, and the optimization technique that was used will be introduced.

4.1 Design variables, constraints and objective functions

The problem consists in maximizing the performance of the system over its lifetime when considering the changes in operating conditions. The objective function that was considered is the total energy produced over the lifetime of the system, i.e., Eq. (19). This objective function differs from the specific power (net power divided by the geofluid mass flowrate) more commonly encountered in literature. In the present case, since the geofluid mass flow rate is also a design variable and is not known a priori, maximizing the specific power would not make sense. In fact, optimal designs could feature a very high specific power with a very low geofluid mass flowrate, and the power plant would end up producing only a small amount of energy each year. Such designs would not be economically viable, as power plants are built to produce energy in the first place. The optimization problem statement is:

$$\begin{gathered} \text{Maximize } (E_{tot}) \\ \text{Optimizing } (P_{high}, \dot{m}_{wf}, r) \\ \text{Respecting } (T_D > 30\ °C,\ P_{high} < 4.06\ MPa,\ T_{cond} > 0\ °C) \\ \text{Respecting (State 5: saturated or superheated gas)} \\ \text{Fixed/known parameters: see Table 1} \end{gathered} \tag{20}$$

The objective is thus to maximize the total energy produced by the power plant during its lifetime by optimizing the evaporator pressure, the geofluid mass flow rate, and the working fluid-to-geofluid flow rate ratio, while respecting the constraints given in Eq. (20). The parameters that need to be specified are listed in the first column of Table 1.

4.2 Optimization technique

The optimization problem was solved with the *fmincon* algorithm from the optimization toolbox available in Matlab [27]. With this approach, an initial point in the design space

needs to be specified. The final optimal result was found to be sensitive to the initial point that was specified. Therefore, a large number of random initial points in the design space (i.e., sets of parameters P_{high}, $\dot{m}_{geo}$, r) were generated. Each set of parameters was simulated and the 5 best were used as initial points for a full optimization. Finally, the best among the formal optimization runs was kept as the final result.

This procedure was tested for different cases for which the optimal design was known from parametric sweeps. It was found that the procedure was able to properly identify the global optimum.

5. Maximization of E_{tot}

5.1 Effect of ratio r

The procedure introduced in Section 4.2 was first used to obtain the maximum energy produced over the power plant lifetime while varying the evaporator pressure and the geofluid mass flow rate for a given mass flow rate ratio r. The other parameters were fixed and kept to the same values as above. In order to illustrate the impact of r on the objective function, the procedure was repeated for different values of r, and the results were reported in Fig. 5. Each point represents a full optimization with respect to the evaporator pressure and geofluid mass flow rate for the specified r-value. One can see that increasing r is beneficial up to a point where the objective function starts to decrease abruptly. Increasing the working fluid mass flow rate (i.e., reducing the ratio r) first tends to increase the power output as it is accompanied by a larger pressure drop at the turbine due to Eq. (13). However, at some point, when the working fluid flow rate increases too much, the pumping power becomes more significant and the temperature of point 4 in Fig. 1 drops too much (i.e., point 4 falls within the bell shape in the T-s diagram), leading to unviable cycles. These competing trends explain the presence of an optimum in Fig. 5.

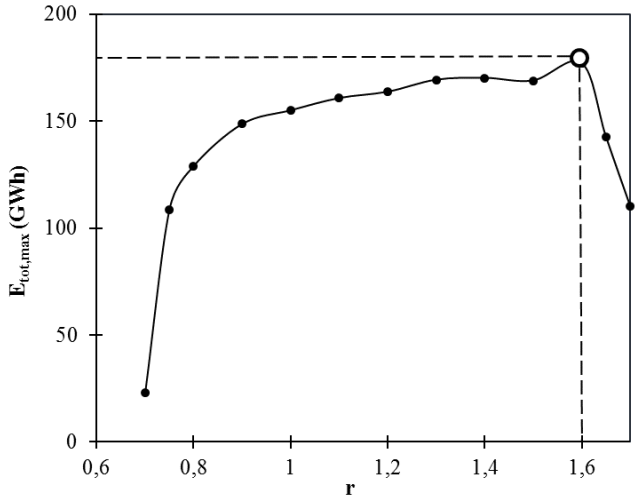

Figure 5

5.2 Impact of evaporator UA-value

In this section, the ratio r was considered as a design variable in the optimization, i.e., the evaporator pressure, geofluid mass flow rate and r-ratio were optimized simultaneously to maximize the total energy produced over the lifetime of the power plant. The optimization was repeated for different evaporator sizes, i.e., different UA-values, in order to understand the influence of this parameter. The UA value is an indication of the size and cost of the evaporator.

One can observe in Fig. 6 the presence of an optimum, i.e., a value of UA that maximizes the total energy production. This result might look surprising since when the heat exchanger becomes larger, one usually expects more heat to be recovered from the geofluid and thus, more energy produced. To develop a better understanding of this result, the optimized design variables are shown in Fig. 7 as a function of the UA-value. Fig. 7 reveals that the optimized geofluid flow rate increases at low UA-values, which is coherent with the idea that a larger heat exchanger can handle a larger mass flow rate. However, increasing UA beyond a certain value eventually results in a geothermal reservoir that cools down too rapidly and yields unviable cycles at the end of the power plant lifetime (e.g., point 4 inside the T-s bell shape). Consequently, the optimization process at large UA-values tends to decrease the geofluid flow rate to produce thermodynamic cycles that can work properly throughout their entire lifetime. In other

words, the optimized cycles at large UA-values need to operate at reduced geofluid flow rate in order to be able to work properly for the entire lifetime of the plant. This is obviously detrimental to the net power output during the first years of operation, but it is necessary in order to maximize the total energy produced over the course of the plant's lifetime. Additionally, one can observe in Fig. 7 an overall increase of the optimal evaporator pressure. Note that the optimal ratio r follows a pattern similar to $\dot{m}_{geo}$, as the two variables are linked through Eq. (18).

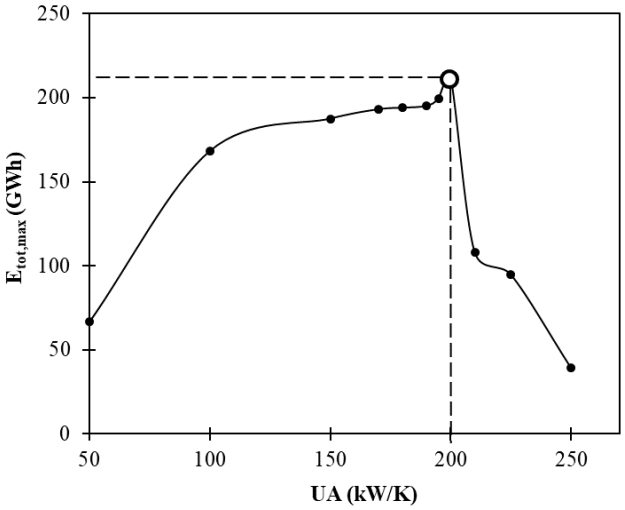

Figure 6

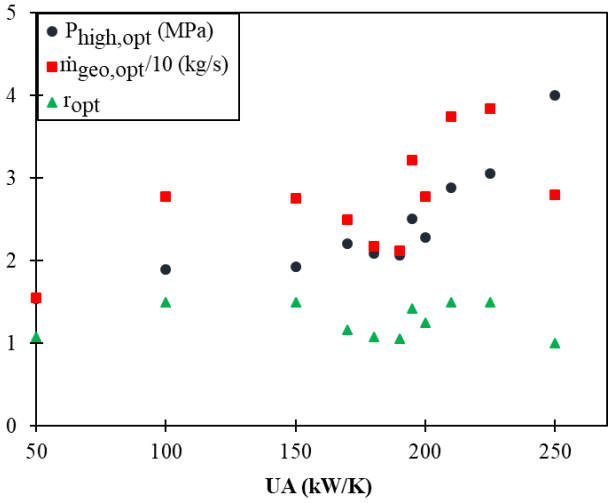

Figure 7

The choice of the right UA-value for a heat exchanger is often seen as the result of an economic trade-off between the initial cost and the operation cost [31–34]. The results of this section suggest, however, that the best UA-value is also dictated in the present case by the finite amount of energy available in the reservoir and by the requirement of the cycle to adapt to evolving conditions. Different examples of optimized cycles as a function of UA are shown in Fig. 8. The first column corresponds to the cycles during their first year of operation while the second column represents the cycles at the end of their lifetime. Note that the T-s diagram of the optimal cycle that yielded the highest value of $E_{tot,max}$ (211.55 GW h) in Fig. 6 is shown in Fig. 8c) and d) with UA=200 kW/K. The working fluid mass flow rates for the three ORCs depicted in Fig. 8 are 18.52, 22.17, and 20.79 kg/s for UA = 100, 200, and 225 kW/K, respectively. As explained previously, when using Eq. (13) to calculate the pressure drop in the turbine, larger mass flow rates result in larger pressure drops (1.56, 1.99, and 1.32 MPa at n=1 and 1.12, 1.32, and 1.02 MPa for n=50, for the three aforementioned cases). Thus, the optimal design in Figs. 6 and 8 is the ORC design that can sustain the largest working fluid mass flowrate and pressure drop in the turbine throughout its entire exploitation period. It is interesting to observe that all optimized cycles in Fig. 8 exhibit a common feature at the end of the plant lifetime (Fig. 8b), d), and f)), i.e., the working fluid at the exit of the turbine is nearly at the saturated vapor state at that time.

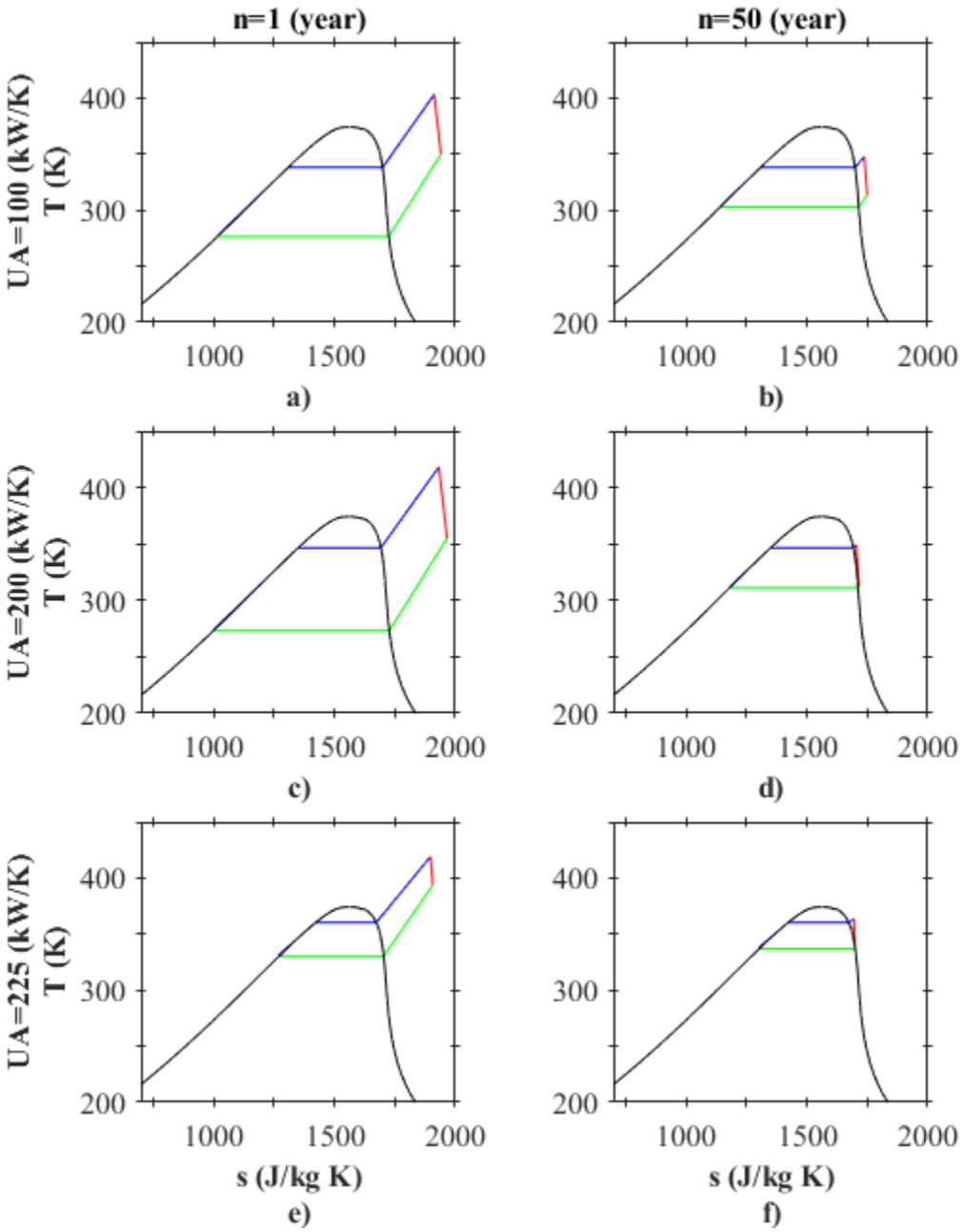

Figure 8

5.3 Impact of turbine constant K

In addition to the evaporator, another important piece of equipment is the turbine. In the present model, the turbine is characterized by its constant K, which depends on the size and performance of the turbine. A procedure similar to that presented in the previous section was thus implemented. For different values of K, the evaporator pressure,

geofluid mass flow rate and flow ratio were optimized simultaneously in order to maximize the energy output of the plant over its lifetime. Other parameters, such as the UA-value, were kept constant. Results are shown in Fig. 9.

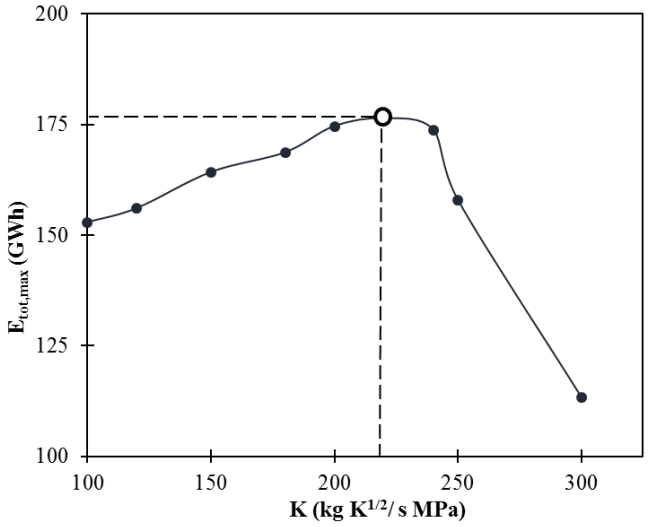

Figure 9

An optimal K-value was identified. Increasing K tends to increase the pressure drop in the turbine, and thus the power output. However, when the pressure drop becomes too large, an unviable cycle is generated because the working fluid leaves the turbine (state 5) as a saturated mixture. As a result, the optimization process produces cycles that are not as efficient, but that are viable, which explains the drop of E_{tot} when K becomes larger.

Figure 10 reports the optimal value of the design variables as a function of K. It can be seen that, as opposed to the previous optimization, increasing K has a tendency to decrease the optimal evaporator pressure and slightly increase the geofluid mass flow rate (and mass flow rate ratio, since both follow a similar pattern as mentioned previously).

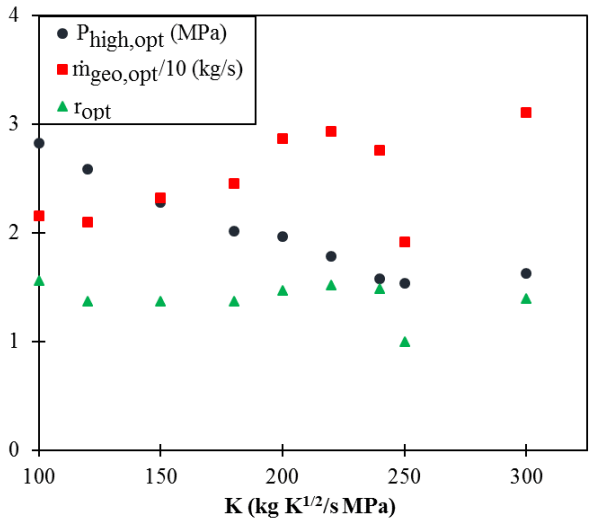

Figure 10

5.4 Effect of power plant lifetime

Finally, the effect of the number of years N over which the power plant works was investigated. For fixed UA_{tot} and K values, the three design variables (i.e., evaporator pressure, geofluid flow rate and flow ratio) were optimized for different values of N. It can be seen in Fig. 11 that the planning and exploitation of the plant over a longer period generates more energy over the course of its lifetime (e.g., ~3 times more energy produced for a plant optimized for a 50 years exploitation compared to a plant optimized for a 10 year exploitation). Note that despite being exploited over a period five times longer, the energy produced by the plant optimized for 50 years is not five times larger. There is thus a diminishing return in using an optimized plant for longer operation periods, as the geothermal reservoir offers a finite amount of energy. In other words, even if the energy produced per year is larger in the case of geothermal power plants optimized over a shorter period, more energy is produced overall by plants optimized for a longer exploitation.

The optimized design variables are shown in Fig. 12 as a function of N. One can observe that the mass flow ratio r is almost unaffected by the lifetime, while the geofluid mass flow rate and the evaporator pressure decrease when the plant is optimized for longer exploitation periods. This can be explained by the fact that larger values of N can lead to unviable cycles near the end of the plant's lifetime for given values of UA and K,

similarly to the case of large UA values discussed in Section 5.2. Thus, in order to respect all the constraints of the optimization, the resulting optimal cycles generally produce less energy but can work for the entire operation period.

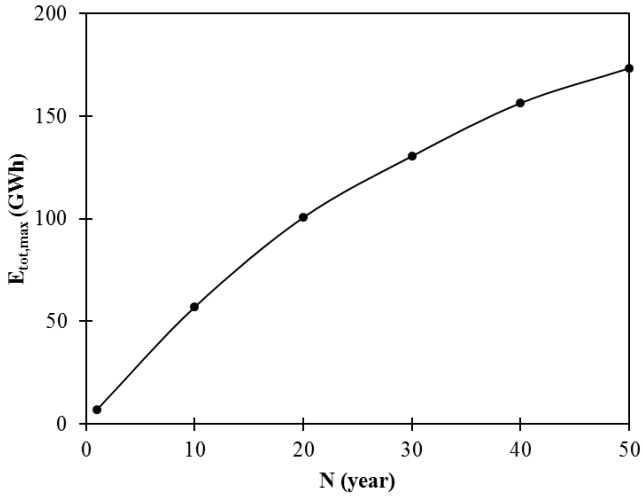

Figure 11

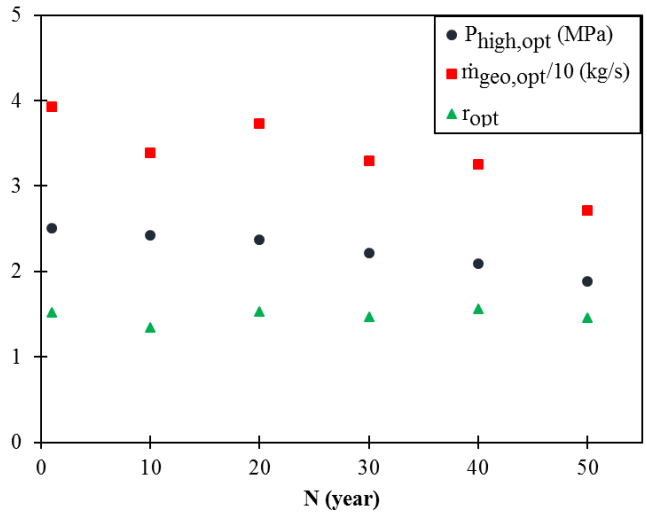

Figure 12

6. Comparison of optimization under varying versus steady-state conditions

In the previous section, the cycle was optimized while considering that the operation conditions changed over time. As mentioned in the introduction, thermodynamic cycles for geothermal power plants are often optimized under steady-state conditions. It is thus

instructive to compare these two approaches, i.e., optimization performed in steady-state versus transient conditions, as the former approach is more often used in literature as opposed to the latter.

For the reference case that was analyzed in the previous sections, the cycle was thus optimized again, this time considering only one fixed inlet geofluid temperature (i.e., steady-state conditions). The optimization was performed for three different values of inlet geofluid temperatures: (i) initial temperature of the reservoir, (ii) expected end of lifetime reservoir temperature and (iii) mid-life expected temperature.

In Table 2, one can find the optimized parameters of the cycles achieved while assuming a constant geofluid temperature, as well as the cycle optimized from the start with the transient evolution of the reservoir.

Table 2. Parameters of optimized cycles assuming a constant geofluid inlet temperature vs. the actual geofluid temperature evolution, and energy produced over the geothermal power plant lifetime with these cycles.

T_{res} for optimization (K)	$P_{high,opt}$ (MPa)	$\dot{m}_{geo,opt}$ (kg/s)	r_{opt} (-)	$E_{tot,max}$ (GWh)
422	2.75	42.10	1.46	332
402	2.00	25.12	1.18	241
386	1.54	18.91	1.15	171
Transient conditions	1.89	27.77	1.50	168

As the assumed steady-state temperature of the geofluid increases, the optimized evaporator pressure, geofluid flow rate and mass ratio all increase, which is coherent with the results often reported in literature [36]. It is worth to note that the cycle that was optimized by simulating the transient evolution of the geothermal reservoir (i.e., last line of Table 2) produced less energy than the predicted by the first three optimizations at constant geofluid temperature. In other words, if the transient conditions are completely ignored and T_{res} is considered constant during the entire lifetime of the plant (steady-state

conditions), the total energy output of the plant is over-estimated regardless of the choice for the design reservoir temperature. This emphasizes the relevance of the approach proposed in this paper to optimize geothermal power plants by considering their lifetime evolution. If, nevertheless, a steady-state optimization was considered, the expected end of lifetime reservoir temperature appears to be a reasonable assumption in the present case (differences of ~2% for the energy produced and between 17% and 23% for the other optimized design variables when compared to an optimization that considers transient operating conditions).

7. Optimal cycles with evolving design

In the previous sections, the evaporator pressure, geofluid mass flow rate, and mass flow rate ratio r were assumed to be constant throughout the entire exploitation period of the plant for the purpose of the optimization process. In this section, this assumption is relaxed and the parameters of the optimization are allowed to change with time. In order to limit the number of design variables, this is achieved by assigning values for each of the three parameters both at the beginning and at the end of the lifetime of the plant while assuming a linear variation for intermediate times. Therefore, a total number of 6 design variables are now considered for this optimization.

Table3. Comparison of the optimization results assuming constant design variables as a function of time (evaporator pressure, geofluid mass flow rate and flow rate ratio) vs. assuming time-varying design variables, for the reference case.

	$P_{high,opt}$ (MPa)		$\dot{m}_{geo,opt}$ (kg/s)		r_{opt} (-)		$E_{tot,max}$ (GWh)
	(n=1)	(n=50)	(n=1)	(n=50)	(n=1)	(n=50)	
Time-varying design variables	2.03	1.54	26.44	22.07	1.30	1.37	220
Constant design variables	1.89		27.77		1.50		168

The results of this optimization are reported in Table 3 for the reference case with constant parameters (see Table 1 for the relevant parameters), as well as for the same case under the assumption of a linear variation of the design variables in time. The total energy obtained for the optimal plant with variable parameters is 220 GWh (as opposed to 168 GWh for constant parameters), which represents an improvement ~31% over the entire lifetime of the plant. To better understand the major factors responsible for this improvement, the T-s diagrams of both cycles are shown in Fig. 13, where the red and blue cycles refer to the optimizations performed with time-varying and constant design variables, respectively. By recognizing that the total work done by a cycle is given by the area inside each cycle in Fig. 13, it can be observed that the cycle with constant parameters produces slightly more work but only at the beginning of the exploitation period (see Fig. 13a as compared to Fig. 13b and c). Even then, since the working fluid mass flow rate is higher for the cycle with time-varying parameters (20.34 kg/s as opposed to 18.51 kg/s), it produces more power even during the first years. Overall, the optimization with time-varying parameters results in a cycle that produces more net power at every year as can be seen in Fig. 14 and thus, it also produces more energy over the course of its exploitation.

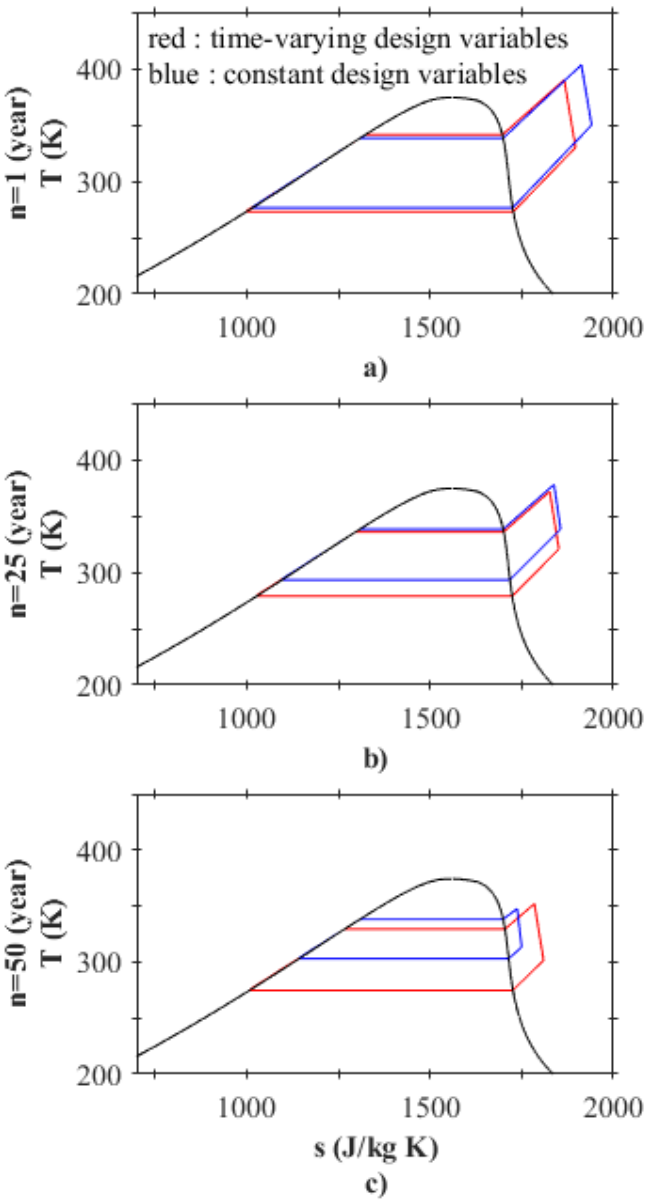
red : time-varying design variables
blue : constant design variables
n=1 (year)
T (K)
400
300
200
1000
1500
2000
a)
n=25 (year)
T (K)
400
300
200
1000
1500
2000
b)
n=50 (year)
T (K)
400
300
200
1000
1500
2000
s (J/kg K)
c)

Figure 13

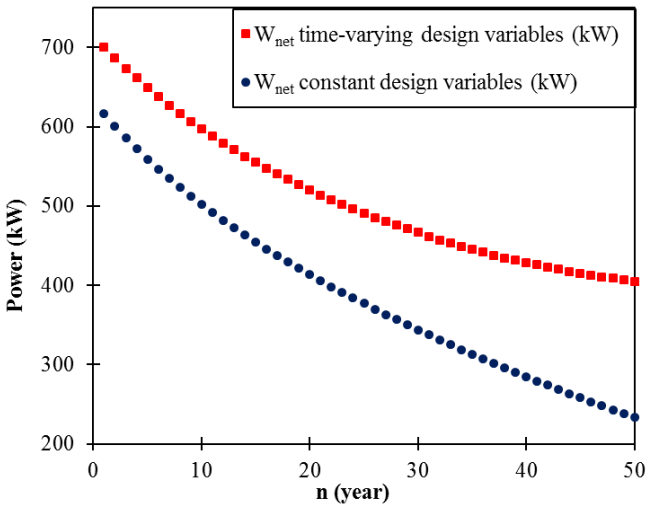

Figure 14

8. Conclusions

In this work, a framework for the optimization of geothermal power plants while considering the transient evolution of the reservoir properties was laid out. A simplified thermal reservoir model was introduced, which allowed a coupling between the plant and the reservoir models. By performing a series of parametric sweeps, it was possible to identify the impact of key parameters in the design and optimization of geothermal plants for evolving operating conditions. Note that the optimization approach explained in Section 4 was found to be very sensitive to the initial guess made for the design variables. It was observed that different combinations of the design variables could lead to near-optimal designs (local minima) that produced nearly the same amount of energy over the exploitation period of the power plant. There are thus great opportunities to improve the overall optimization procedure for the problem studied in the present paper which featured a limited design space due to the presence of many constraints.

It was demonstrated that increasing the size of the evaporator heat exchanger (through its UA-value) led to more total energy produced by the plant (E_{tot}) over the course of its exploitation. However, increasing UA beyond a certain point led to a drop of power output, as the plant eventually depleted the thermal reservoir and could not produce any energy near the end of its lifetime. Similar behavior were observed for the working fluid to geofluid mass flow rate ratio and the turbine constant K. For these

parameters, however, the thermodynamic cycles that were viable during the entire plant lifetime (i.e., cycles with physically realistic behavior) produced less energy overall.

In the last sections of this paper, optimal designs were compared with designs resulting from steady-state optimization runs, i.e., runs where the geothermal reservoir properties were constant and equal to either initial, final, or midlife values. The main outcome of this comparative exercise was that all steady-state optimizations that assumed a constant thermal reservoir temperature led to an over-estimation of the energy produced by the power plant throughout its lifetime (98%, 45%, and 2% more energy produced when using the initial, expected mid-life, and expected end of life temperatures, respectively). The constant thermal reservoir temperature that yielded an energy output closest to the case that considered the time-evolution of the thermal reservoir was the expected end of life temperature. It was also demonstrated that the energy output could be increased significantly (~31% over the entire lifetime of the plant) if the operating conditions (mass flow rate ratio, geofluid mass flow rate, and pressure at the evaporator) were allowed to change over the course of the plant's lifespan.

This work could be seen as a first step towards a complete thermodynamic-hydrogeological integrated optimization model. Future work could include coupling with more advanced geothermal reservoir models with underground flows, fracture networks, different soil layers, etc. The power plant model itself could also be improved, and new design parameters could be addressed, such as the sizing of the condenser and the optimization of the working fluid which could also be a mixture [37]. Other objectives functions could be considered in future work [38], such as energy and exergy efficiency, cost, environmental footprint, etc. The opportunity to create a synergy between a geothermal power plant and other facilities (e.g., liquid natural gas [39], hydrogen production [40], etc.), while considering the depletion of the reservoir, could also be interesting. Finally, it could be interesting to assess the viability of changing some of the power plant components (turbine, pumps, etc.) during its lifetime, both in terms of energy and economic perspectives.

Acknowledgements

The authors' work was supported by a Cooperative Research and Development (CRD) Grant of the Natural Sciences and Engineering Research council of Canada (NSERC) and by the Institut de recherche d'Hydro-Québec (IREQ).

References

[1] A. Hussain, S. M. Arif, and M. Aslam, “Emerging renewable and sustainable energy technologies: State of the art,” *Renew. Sustain. Energy Rev.*, vol. 71, pp. 12–28, May 2017.

[2] R. Bertani, “Geothermal power generation in the world 2005-2010 update report,” *Geothermics*, vol. 41, pp. 1–29, Jan. 2012.

[3] “Technology Roadmap: Geothermal Heat and Power,” International Energy Agency, 75739 Paris Cedex 15, France, 2011.

[4] A. Evans, V. Strezov, and T. J. Evans, “Assessment of sustainability indicators for renewable energy technologies,” *Renew. Sustain. Energy Rev.*, vol. 13, no. 5, pp. 1082–1088, Jun. 2009.

[5] C. Tomasini-Montenegro, E. Santoyo-Castelazo, H. Gujba, R. J. Romero, and E. Santoyo, “Life cycle assessment of geothermal power generation technologies: An updated review,” *Appl. Therm. Eng.*, vol. 114, pp. 1119–1136, Mar. 2017.

[6] J. I. Martinez-Corona, T. Gibon, E. G. Hertwich, and R. Parra-Saldivar, “Hybrid life cycle assessment of a geothermal plant: From physical to monetary inventory accounting,” *J. Clean. Prod.*, vol. 142, pp. 2509–2523, Jan. 2017.

[7] I. A. Thain and B. Carey, “Fifty years of geothermal power generation at Wairakei,” *Geothermics*, vol. 38, no. 1, pp. 48–63, Mar. 2009.

[8] N. Rman, A. Lapanje, J. Prestor, and M. J. O’Sullivan, “Mitigating depletion of a porous geothermal aquifer in the Pannonian sedimentary basin,” *Environ. Earth Sci.*, vol. 75, no. 8, Apr. 2016.

[9] C. J. Bromley, “Groundwater changes in the Wairakei–Tauhara geothermal system,” *Geothermics*, vol. 38, no. 1, pp. 134–144, Mar. 2009.

[10] R. C. Gunasekera, G. R. Foulger, and B. R. Julian, “Reservoir depletion at The Geysers geothermal area, California, shown by four-dimensional seismic tomography: Reservoir depletion shown by 4-D tomography,” *J. Geophys. Res. Solid Earth*, vol. 108, no. B3, Mar. 2003.

[11] R. Gabbrielli, “A novel design approach for small scale low enthalpy binary geothermal power plants,” *Energy Convers. Manag.*, vol. 64, pp. 263–272, décembre 2012.

[12] F. Heberle, C. Schifflechner, and D. Brüggemann, “Life cycle assessment of Organic Rankine Cycles for geothermal power generation considering low-GWP working fluids,” *Geothermics*, vol. 64, pp. 392–400, Nov. 2016.

[13] R. DiPippo, “Second Law assessment of binary plants generating power from low-temperature geothermal fluids,” *Geothermics*, vol. 33, no. 5, pp. 565–586, Oct. 2004.

[14] K. A. Barse and M. D. Mann, “Maximizing ORC performance with optimal match of working fluid with system design,” *Appl. Therm. Eng.*, vol. 100, pp. 11–19, May 2016.

[15] H. D. Madhawa Hettiarachchi, M. Golubovic, W. M. Worek, and Y. Ikegami, “Optimum design criteria for an Organic Rankine cycle using low-temperature geothermal heat sources,” *Energy*, vol. 32, no. 9, pp. 1698–1706, Sep. 2007.

[16] A. Ergun, M. Ozkaymak, G. Aksoy Koc, S. Ozkan, and D. Kaya, “Exergoeconomic analysis of a geothermal organic Rankine cycle power plant using

the SPECO method," *Environ. Prog. Sustain. Energy*, vol. 36, no. 3, pp. 936–942, May 2017.
[17] V. Zare, "A comparative exergoeconomic analysis of different ORC configurations for binary geothermal power plants," *Energy Convers. Manag.*, vol. 105, pp. 127–138, Nov. 2015.
[18] X. Liu, Y. Zhang, and J. Shen, "System performance optimization of ORC-based geo-plant with R245fa under different geothermal water inlet temperatures," *Geothermics*, vol. 66, pp. 134–142, Mar. 2017.
[19] F. Alobaid, N. Mertens, R. Starkloff, T. Lanz, C. Heinze, and B. Epple, "Progress in dynamic simulation of thermal power plants," *Prog. Energy Combust. Sci.*, vol. 59, pp. 79–162, Mar. 2017.
[20] K. Indriawati, G. Nugroho, B. L. Widjiantoro, and T. R. Biyanto, "Study of plant-wide control implementation in production process of geothermal power plant," *J. Eng. Sci. Technol.*, vol. 12, no. 2, pp. 333–348, 2017.
[21] D. S. Pamuji, Sihana, and K. Suryopratomo, "Thermodynamic analysis of the effect of reservoir temperature change on the performance of organic rankine cycle system on geothermal power plant," 2016, p. 110005.
[22] G. Axelsson, G. Björnsson, and F. Gudni Axelsson, Grímur Björnsson and Francisco Montalvo, "Quantitative Interpretation of Tracer Test Data," in *Proceedings World Geothermal Congress*, 2005, pp. 24–29.
[23] D. Budisulistyo, C. S. Wong, and S. Krumdieck, "Lifetime design strategy for binary geothermal plants considering degradation of geothermal resource productivity," *Energy Convers. Manag.*, vol. 132, pp. 1–13, Jan. 2017.
[24] J. Majorowicz and V. Minea, "Geothermal energy potential in the St-Lawrence River area, Québec," *Geothermics*, vol. 43, pp. 25–36, Jul. 2012.
[25] P. Amatyakul *et al.*, "Exploring the shallow geothermal fluid reservoir of Fang geothermal system, Thailand via a 3-D magnetotelluric survey," *Geothermics*, vol. 64, pp. 516–526, Nov. 2016.
[26] F. P. Incropera, D. P. DeWitt, T. L. Bergman, and A. S. Lavine, *Fundamentals of Heat and Mass Transfer*, 6th ed. John Wiley & Sons, Inc., 2007.
[27] *MATLAB and Optimization Toolbox 7.0 Release 2014a, The Mathworks, Inc.* Natick, Massachusetts, United States.
[28] A. Rivera Diaz, E. Kaya, and S. J. Zarrouk, "Reinjection in geothermal fields: A worldwide review update," *Renew. Sustain. Energy Rev.*, vol. 53, pp. 105–162, Jan. 2016.
[29] A. Chaibakhsh and A. Ghaffari, "Steam turbine model," *Simul. Model. Pract. Theory*, vol. 16, no. 9, pp. 1145–1162, Oct. 2008.
[30] Y. A. Cengel and M. A. Boles, *Thermodynamics: An Engineering Approach*, 7th ed. New-York: McGraw-Hill, 2011.
[31] N. Chagnon-Lessard, F. Mathieu-Potvin, and L. Gosselin, "Geothermal power plants with maximized specific power output: Optimal working fluid and operating conditions of subcritical and transcritical Organic Rankine Cycles," *Geothermics*, vol. 64, pp. 111–124, Nov. 2016.
[32] M. Asadi, Y. Song, B. Sunden, and G. Xie, "Economic optimization design of shell-and-tube heat exchangers by a cuckoo-search-algorithm," *Appl. Therm. Eng.*, vol. 73, no. 1, pp. 1032–1040, Dec. 2014.

[33] M. Fesanghary, E. Damangir, and I. Soleimani, “Design optimization of shell and tube heat exchangers using global sensitivity analysis and harmony search algorithm,” *Appl. Therm. Eng.*, vol. 29, no. 5–6, pp. 1026–1031, Apr. 2009.
[34] A. C. Caputo, P. M. Pelagagge, and P. Salini, “Heat exchanger design based on economic optimisation,” *Appl. Therm. Eng.*, vol. 28, no. 10, pp. 1151–1159, Jul. 2008.
[35] R. Selbaş, Ö. Kızılkan, and M. Reppich, “A new design approach for shell-and-tube heat exchangers using genetic algorithms from economic point of view,” *Chem. Eng. Process. Process Intensif.*, vol. 45, no. 4, pp. 268–275, Apr. 2006.
[36] J. Clarke and J. T. McLeskey, “Multi-objective particle swarm optimization of binary geothermal power plants,” *Appl. Energy*, vol. 138, pp. 302–314, Jan. 2015.
[37] K. Satanphol, W. Pridasawas, and B. Suphanit, “A study on optimal composition of zeotropic working fluid in an Organic Rankine Cycle (ORC) for low grade heat recovery,” *Energy*, vol. 123, pp. 326–339, Mar. 2017.
[38] J. Varney, S. J. Zarrouk, N. Bean, and B. Bendall, “Performance measures in geothermal power developements,” *Renew. Energy*, vol. 101, pp. 835–844, Feb. 2017.
[39] A. H. Mosaffa, N. H. Mokarram, and L. G. Farshi, “Thermo-economic analysis of combined different ORCs geothermal power plants and LNG cold energy,” *Geothermics*, vol. 65, pp. 113–125, Jan. 2017.
[40] M.-E. Ramazankhani, A. Mostafaeipour, H. Hosseininasab, and M.-B. Fakhrzad, “Feasibility of geothermal power assisted hydrogen production in Iran,” *Int. J. Hydrog. Energy*, vol. 41, no. 41, pp. 18351–18369, Nov. 2016.

Figure captions

Figure 1 Schematic representation of the geothermal power plant.

Figure 2 T-s diagram of the power cycle and evolution from the beginning to the end of life for the reference case.

Figure 3 Energy produced over the plant lifetime (E_{tot}) as a function of the geofluid mass flow rate and evaporator pressure, with r=1 and other parameters as in Table 1.

Figure 4 Evolution of power produced by the turbine, used by the pump and net power over the lifetime for the reference case.

Figure 5 Energy produced over the plant lifetime ($E_{tot,max}$) with optimization of the geofluid mass flow rate and evaporator pressure as a function of ratio r.

Figure 6 Energy produced over the plant lifetime ($E_{tot,max}$) with optimization of the geofluid mass flow rate, the evaporator pressure and the ratio r as a function of UA.

Figure 7 Values of the optimal geofluid mass flow rate, evaporator pressure and ratio r as a function of UA.

Figure 8 Optimized cycles at the beginning and at the end of the lifetime for UA=100 kW/m^{2}K, UA=200 kW/m^{2}K, and UA=225 kW/m^{2}K.

Figure 9 Energy produced over the plant lifetime ($E_{tot,max}$) with optimization of the geofluid mass flow rate, the evaporator pressure and the ratio r as a function of K.

Figure 10 Values of the optimal geofluid mass flow rate, evaporator pressure and ratio r as a function of K.

Figure 11 Energy produced over the plant lifetime ($E_{tot,max}$) with optimization of the geofluid mass flow rate, the evaporator pressure and the ratio r as a function of the lifetime N considered.

Figure 12 Values of the optimal geofluid mass flow rate, evaporator pressure and ratio r as a function of N.

Figure 13 Comparison of the T-s diagrams of the power plants optimized with time-varying or constant design variables at different times during their exploitation.

Figure 14 Net power produced by the power plants optimized with time-varying or constant design variables as a function of time.

Table captions

Table 1 Values of the model parameters for the reference case.

Table 2 Parameters of optimized cycles assuming a constant geofluid inlet temperature vs. the actual geofluid temperature evolution, and energy produced over the geothermal power plant lifetime with these cycles.

Table3 Comparison of the optimization results assuming constant design variables as a function of time (evaporator pressure, geofluid mass flow rate and flow rate ratio) vs. assuming time-varying design variables, for the reference case.